REMUNOM
ISSN 2178-6925

Received: 05/03/2026 - **Accepted:** 06/05/2026
Vol: 13.07
DOI: 10.66104/m4ev7706
Pages: 1-20

ANALYSIS OF THE TRUE STRAIN OF CONVENTIONAL SAE1010 STEEL IN THE AIR BENDING PROCESS

Valtenês de Souza Bossle
Federal University of Rio Grande do Sul, Brazil
E-mail: valtenes.bossle@gmail.com

Lirio Schaeffer
Federal University of Rio Grande do Sul, Brazil
E-mail: schaefer@ufrgs.br

Matheus Henrique Riffel
Federal University of Rio Grande do Sul, Brazil
E-mail: matheus.riffel@ufrgs.br

Rafael Pandolfo da Rocha
Federal University of Rio Grande do Sul, Brazil
E-mail: rafael.pandolfo@ufrgs.br

Juliano Cantarelli Toniolo
Federal Institute of Education, Science and Technology of Rio Grande do Sul, Brazil
E-mail: juliano.toniolo@caxias.ifrs.edu.br

Abstract

Determining the True Strain in the air bending process is of fundamental importance for predicting possible failures in the bent region of the formed part. Among steels classified as conventional, SAE1010 is used in the manufacture of parts for a wide variety of market segments. This study aims to evaluate mathematical equations for calculating the True Strain in the outer fibers of the bending region that occur in the air bending process for this steel and compare them with the results of scientific work obtained for AHSS S900MC steel, through analytical calculation methods and computer simulation, comparing them with results obtained through experimental analyses. Four punches were used, varying for each one the distance between the die supports and the punch displacement. It was verified through experimental analysis that the measured values of True Strain are different in the outer fibers of the bending region. However, it was found that the values obtained through analytical calculation methods for conventional SAE1010 steel are the same as those verified

REMUNOM
ISSN 2178-6925

Received: 05/03/2026 - **Accepted:** 06/05/2026
Vol: 13.07
DOI: 10.66104/m4ev7706
Pages: 1-20

for AHSS S900MC steel, despite the materials having peculiar mechanical properties. The predictability, through the analytical method, in relation to the experimental values of the True Strain for conventional SAE1010 steel ranged from -25.7% to 8.3%.

Keywords: True Strain, air bending process, conventional SAE1010 steel.

1. Introduction

Among steels classified as conventional (ULSAB, 2017), the SAE1010 grade, with commercial quality, has a Maximum Stress (R_m) of 365 MPa and this steel is used in bending processes in the automotive industry, appliance, general industries, and is occasionally used in the stamping of shallow parts with simple geometries (Bossle et al., 2025).

Conventional SAE1010 carbon steel is widely used in the manufacture of the most varied types of parts due to its low cost and physical and chemical characteristics. Among carbon steels, this is the most common due to its ease of manufacture, good weldability, and mechanical properties (Almeida, 2021).

The True Strain (φ_x) during the air bending process results in an elastic-plastic strain in the bending region. In this region, the outer zone of the material is elongated, resulting in tensile strain, while the inner zone is compressed, resulting in compressive strain, as shown in Figure 1 (Oehler and Kaiser, 1993; Kluge, 2020).

Figure 1: Representation of strains in the bending region.

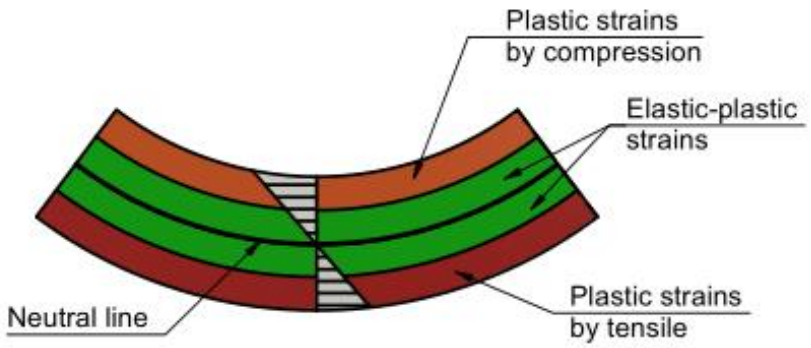

Source: Elaborated by authors (2026).

One of the difficulties in the mechanical forming process of high-strength steel

REMUNOM
ISSN 2178-6925

Received: 05/03/2026 - **Accepted:** 06/05/2026
Vol: 13.07
DOI: 10.66104/m4ev7706
Pages: 1-20

sheets, due to their low deformability, is avoiding the appearance of cracks and fissures in the in the bending region (Perka, 2022).

In the bending region obtained through the air bending process, the material creates a narrow elastic band on both sides of the neutral line, and as it moves away towards the surface, stresses above the yield strength are obtained, causing permanent plastic strain. When the punch moves away, the elastic band tends to return to its original flat condition, but this is not possible due to the restrictions caused by the plastic strain zones (Perka, 2022).In the air bending process, the highest value of both stresses occurs on the surface of the material and decreases as it approaches the center of the sheet thickness, becoming zero when it reaches the neutral axis. The strain distribution in air bending process is not symmetrical with respect to the center of the piece. Tensile strains in the outer region are greater than compressive strains in the inner region (Hosford and Caddell, 2011; Schaeffer et al., 2017).

In the air bending process, determining the True Strain (φ_x) is of essential importance, thereby avoiding possible defects such as cracks and fissures in the bending region, as well as ensuring dimensional accuracy and production optimization (Tschätsch, 1997; Kluge, 2020).

Correctly determining the True Strain (φ_x) prevents exceeding the material's ductility limit, especially in parts manufactured with high-strength steel sheets and small Punch Radius (r_p), thus preventing the appearance of cracks and fissures during the air bending process (Çapar, 2026). One of the challenges for the mechanical forming process of metal sheets from high strength steels is to achieve the predictability of the True Strain (φ_x) in the bending zone (Tschätsch, 1997; Mithu et al., 2025).

A few parameters of the air bending process such as Sheet thickness (s), Punch Radius (r_p), Bending Force (F_d), Distances between supports (w) and Maximum Displacement of the Punch (h), as well as some properties of the material such as Anisotropy Index (r), Hardening Coefficient (n), microstructural aspect and lubrication conditions, among others, influenced the strains. (Oehler and Kaiser, 1993; Hosford and Caddell, 2011). Figure 2 shows schematics with air bending

REMUNOM
ISSN 2178-6925

Received: 05/03/2026 - **Accepted:** 06/05/2026
Vol: 13.07
DOI: 10.66104/m4ev7706
Pages: 1-20

process and the main parameters involved in this type of Bending (Aerens and Masselis, 2000; Livatyali and Altan, 2001).

Figure 2: Shows air bending process and the main parameters of this process.

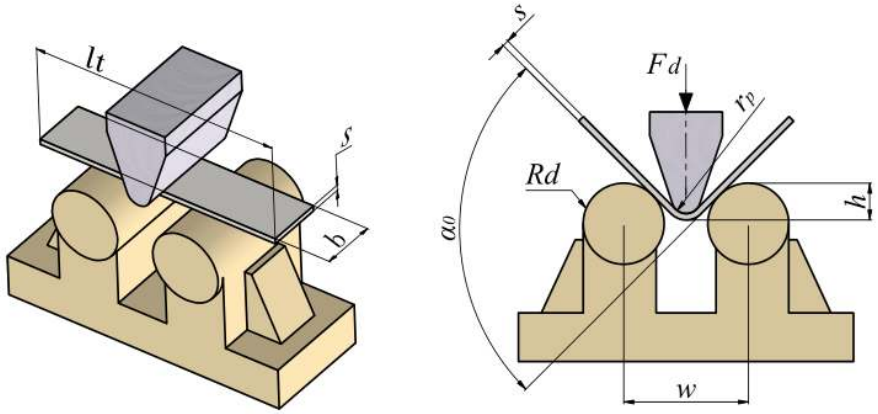

Source: Elaborated by authors (2026).

During the sheet metal forming process, continuous transformations occur in the geometry of the bending region of the part, especially for materials that resist large plastic strains. It is necessary to determine the True Strain (φ_x) to predict and compensate for the springback that occurs after the removal of the Bending Force (F_d), ensuring that the Bending angle after springback (α_1) corresponds to the design angle of the part (Oehler and Kaiser, 1993; Farsi and Arezoo, 2011).

The Force required to bend a sheet depends on the specific operating conditions of each bending process, according to its particularities, and for the air bending process, the Bending Force (F_d) depends on the parameters represented in Figure 2 and the mechanical properties of the material to be bending (Rodrigues and Martins, 2010).

When empirical knowledge is used to determine the parameters of the bending process and to develop the tooling, the cost may be higher and more time may be required, compared to analytical methods or those that use software to perform computational simulation, which become important in the planning and development of tool design (Vorkov, 2018).

This study aims to evaluate the use of analytical expressions in determining the True Strain (φ_x) in the outer bending zone and in the length direction (x) of the

REMUNOM
ISSN 2178-6925

Received: 05/03/2026 - **Accepted:** 06/05/2026
Vol: 13.07
DOI: 10.66104/m4ev7706
Pages: 1-20

sheet, in the air bending process for the SAE1010 conventional steel and compare with the results for AHSS S900MC steel obtained from the work done by Bossle et al. (2026).

Currently, due to its low cost and the quickly obtained results in supporting the performance and optimization of manufacturing projects, the analytical method is still frequently used. (Arola et al., 2015; Schaeffer et al., 2017; Bossle et al., 2026).

2. Methodology

2.1 Determination of the mechanical properties

Table 1 presented the mechanical properties of conventional SAE1010 steel used in this work, in which a tensile test was performed utilizing 9 tests specimens manufactured of this steel with 3.0 mm Sheets thickness (*s*).

Table 1: Mechanical properties of conventional SAE 1010 steel.

Engineering Yield Stress, σ_e (MPa)	Maximum Stress, R_m (MPa)	Relative strain, ε (%)	Elasticity Modulus, *E* (GPa)
241.78	343.56	30.86	198.57

Source: Elaborated by authors (2026).

The dimensions and geometry used for the test specimens were of the rectangular type, and are in accordance with the requirement of ABNT NBR 6892-1:2013 standards, as well as of the procedures to carry out this test. The equipment utilized to perform the tensile test was a 100 kN universal test equipment of the EMIC brand.

The flow stress equation of conventional SAE1010 steels were determined according to the proposal of Ludwik-Hollomon, utilizing the data of Maximum Stress (R_m) and of the respective Relative Strain (ε) corresponding to this point. After this the True Stresses (kf) and True Strains (φ) were calculated using Equations 1 and 2 (Lange, 1985; Bossle et al., 2025).

$$kf = \sigma(1 + \varepsilon) \quad \text{Eq. 1}$$

$$\varphi = \ln(1 + \varepsilon) \quad \text{Eq. 2}$$

REMUNOM
ISSN 2178-6925

Received: 05/03/2026 - **Accepted:** 06/05/2026
Vol: 13.07
DOI: 10.66104/m4ev7706
Pages: 1-20

Equation 3 of Ludwik-Hollomon was used, into which the values of the Hardening Index (*n*), True Strain (φ) and True Stress (kf), were inserted, corresponding to the point of Maximum Stress (R_m) and the respective Relative Strain (*ε)*, and then the values of the Material Resistance Constant (*C*) of this material was determined. Thus, Equation 4 was determined, which describe the Flow Stress Curve of this steel.

Ludwik-Hollomon equation	$kf = C.\varphi^n$	Eq. 3
Conventional SAE1010 steel	$kf = 589.24.\varphi^{0,19}$	Eq. 4

2.2 Methods of analysis

2.2.1 Experimental analysis

To perform the bending experiment, 36 tests specimens were manufactured from conventional SAE1010 steel, utilizing 3mm Sheets thickness (*s*).

For conventional SAE 1010, as it is classified as conventional low-carbon steel, according to the DIN 9635 standard, which states that for conventional low-carbon steels, the Minimum Bending radius (r_{min}) can be 1 to 3 times the initial thickness of the sheet (s_0).

The values of Maximum Displacement of the Punch (*h*) were obtained through a geometrical representation, utilizing the INVENTOR software, where the 4 Punch Radius (r_p) and the 90° Bending angle before springback (α_0). For each Punch Radius (r_p), the Distance between the Supports (*w*) and the Maximum Displacement of the Punch (*h*) varied, and for all representations the Die Radius (R_d) and the thickness of the Sheet thickness (*s*) were equal. Figure 2 is the schematic representation of the air bending experiment. The Distance between the Supports (*w*) was determined using Equation 5, which is adapted from the ABNT NBR 7438:2022 Standard (Bossle et al.,2026).

$$w = (2 * r_p) + (3 * s) + (2 * R_d) \quad \text{Eq. 5}$$

Table 2 shows the values of Distance between the Support (*w*) and Maximum

REMUNOM
ISSN 2178-6925

Received: 05/03/2026 - **Accepted:** 06/05/2026
Vol: 13.07
DOI: 10.66104/m4ev7706
Pages: 1-20

Displacement of the Punch (*h*) for each Punch Radius (r_p) and the Table 3 shows the fixed parameters utilized in the air bending experiment (Bossle et al., 2025).

Table 2: – Values of Maximum Displacement of the Punch (h) and the Distance Between the Supports (w) for each Punch Radius (r_p).

Material	Punch Radius r_p (mm)	Distance between the Support w (mm)	Maximum Displacement of the Punch *h* (mm)
Conventional SAE1010 steel	3	65	20
	6	71	21
	9	77	23
	12	83	25

Source: Elaborated by authors (2026).

Table 3: Fixed parameters utilized in the air bending experiment.

Sheet thickness (*s*)	3mm
Width of the test specimen (*b*)	30mm
Length of the test specimen (*lt*)	210mm
Punch velocity (*V*)	10 mm/min
Bending angle before Springback (α_0)	90°
Die radius (R_d)	25mm

Source: Elaborated by authors (2026).

Punch radii (r_p) of 3, 6, 9 and 12 mm were used, with 9 specimens used for each punch, to compare the True Strain (φ_x) values in the outer bending region.

Before performing the bending experiment, regular circular meshes with an initial diameter (d_0) of 2.5mm were engraved using a laser cutting machine on the surface of the test specimens, as shown in Figure 3.

Figure 3: Mesh of circles with d_0 of 2.5 mm on the surface of the test specimens.



Source: Elaborated by authors (2026).

For experimental analysis, a universal testing machine of 600 kN from EMIC was used to perform the air bending experiment, as shown in Figure 4. The test specimens were bending, placing the face with the engraved circles against the die supports and opposite the punch.

REMUNOM
ISSN 2178-6925

Received: 05/03/2026 - **Accepted:** 06/05/2026
Vol: 13.07
DOI: 10.66104/m4ev7706
Pages: 1-20

Figure 4: Air bending experiment of one of the test specimens.



Source: Elaborated by authors (2026).

Visioplasticity method of measurement involves superimposing a flexible and transparent ruler, positioning its measurement range to best fit the ellipse with the greatest deformation (Folle et al., 2008).

The True Strain (φ_x) in the outer region of the bending was determined using the visioplasticity method by meshes. This method is widely used in studies of plastic strain (Bossle et al., 2026).

To perform the visioplasticity method, 4 groups of 9 tests specimens were used for each one of Punch Radius (r_p) and the averages for each group were calculated.

As shown in Figure 5, was used a flexible and transparent ruler for the initial diameter (d_0) of 2.5mm and the values on the Elongation scale in percentage (%) correspond to Relative Strain (ε), while the values of the Degree of Strain on a logarithmic scale correspond to True Strain (φ_x) in the outer bending region and in the length direction (x), resulting from the bending experiment.

Figure 5: Flexible and transparent ruler used to measure the True Strain (φ_x).

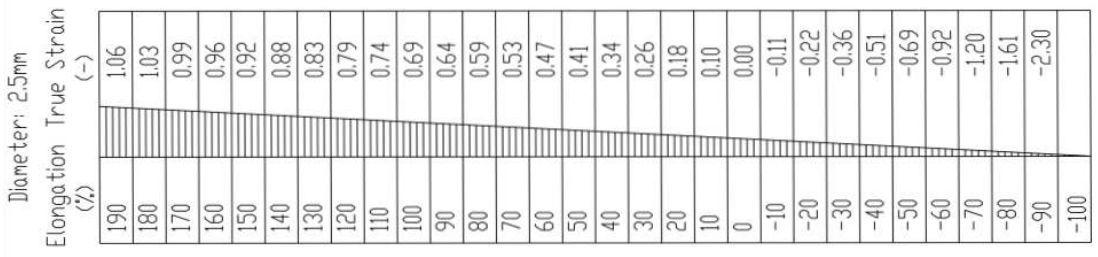

Source: Adapted from Rocha et al. (2023).

The circles with the initial diameter (d_0) deformed, becoming ellipses with a

REMUNOM
ISSN 2178-6925

Received: 05/03/2026 - **Accepted:** 06/05/2026
Vol: 13.07
DOI: 10.66104/m4ev7706
Pages: 1-20

larger dimension (d_x) and a smaller dimension (d_y), as shown in Figure 6.

Figure 6: Representation of the larger (d_x) and smaller (d_y) dimensions of the ellipse in the bending outer region, after the bending experiment. (Adapted from Folle et al., 2008).

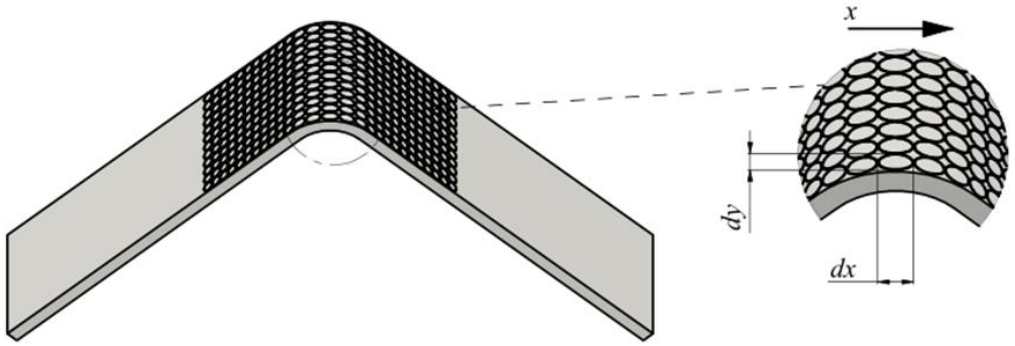

Source: Elaborated by authors (2026).

2.2.2 Analytic methods for calculation

The same parameters of the experimental analysis were utilized in order to perform the analytic calculations using mathematical equations. The True Strains (φ_x) in the outer Zone and in the direction of the sheet length (*x*) as shown in Figure 7, were calculated using Equations 6 proposed by Lange (1985) and 7 proposed by Hosford and Caddell, (2011) that correlates the Sheet thickness (*s*), Punch Radius (r_p), Bending radius of the midline (r_m), the Position of the fibers in the sheet (*y*) as being s/2, the arc length (l_0) and the Length of the fiber (*l*) located in position *y* (Hosford and Caddell, 2011; Bossle et al., 2026).

Figure 7: Representation of the bending region and variables involved in calculating the True Strain (φ_x).

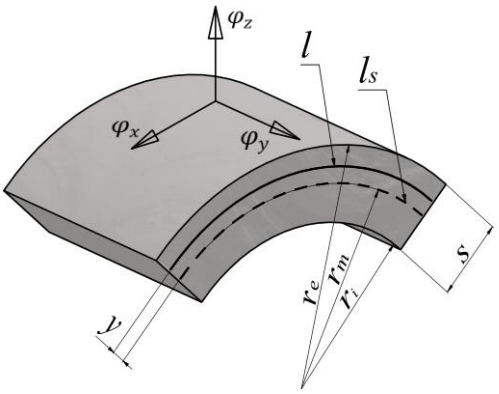

Source: Adapted from Hosford and Caddell (2011).

REMUNOM
ISSN 2178-6925

Received: 05/03/2026 - **Accepted:** 06/05/2026
Vol: 13.07
DOI: 10.66104/m4ev7706
Pages: 1-20

$$\varphi_x = ln\sqrt{1+\frac{s}{r_P}} \qquad \text{Eq. 6}$$

$$\varphi_x = ln\left(1+\frac{s}{2r_m}\right) \qquad \text{Eq. 7}$$

The True Strains (φ_y) in the direction of thickness (*s*) and (φ_z) in the direction of the width (*b*), were not taken into account in this study. Plane Strain was considered, where $\varphi_y = \varphi_x$ e $\varphi_z = 0$ (Vorkov, 2017). On the other hand, Equation 8 was used to calculate the Bending Radius of the midline (r_m), necessary to determine the True Strain (φ_x) (Rocha et al., 2022; Bossle et al., 2026).

$$r_m = r_p + \frac{s}{2} \qquad \text{Eq. 8}$$

2.2.3 Computer simulation

For computer simulations of the air bending process, the SIMUFACT FORMING 15® software (MSC Software Company, Hexagon) was used, with the aim of comparing the results with those of the experimental analysis, and the Finite Element Analysis Method was employed to determine the stress and strain fields along the forming process.

To validate the numerical simulation, 4 of conventional SAE1010 steel bending simulations were performed, one for each Punch Radius (r_p) utilized in the bending experiment, with the aiming to estimate the True Strain (φ_x) in the outer bending region. An elastoplastic formulation suitable for high rotations and moderate deformations was adopted, with a solid-shell discretization, allowing the integration of mechanical variables at multiple points along the sheet thickness (Ledentsoy et al., 2010). The Punches and Die were considered rigid, non-deformable objects, while the sheets were considered elastoplastic objects. The contact between the tool and the sheet was modeled using Coulomb's law of friction, with a constant coefficient of friction μ = 0.1, according to typical conditions of industrial bending

REMUNOM
ISSN 2178-6925

Received: 05/03/2026 - **Accepted:** 06/05/2026
Vol: 13.07
DOI: 10.66104/m4ev7706
Pages: 1-20

processes (Fu et al., 2010; Bossle et al., 2026). The Punch velocity (*V*) was set at 10 mm/min, the same value defined for the bending experiment (Bossle et al., 2026).

The plastic behavior of the material was described by the Ludwik–Hollomon constitutive model, in which the Yield Stress evolves as a function of the equivalent plastic strain according to a power law, adjusted from experimental data. This approach allows for an adequate representation of the material's strain hardening and its influence on bending strength, as well as on the stress distribution along the thickness. The True Strain (φ_x) in the outer bending zone and in the length direction (*x*) of the sheet was evaluated during the punch displacement in the simulation, being determined by the elastic properties and the history of plastic strains imposed during the computer simulation, according to procedures consolidated in the literature on numerical simulation of forming processes (Fu et al., 2010; Hosford and Caddell, 2011; Altan and Tekkaya, 2012; Bossle et al., 2026).

For the simulations, the same sheet thickness (*s*), the same Punch Radii (r_p), the same Distances between Supports (*w*) and the same Punch Displacements (*h*) utilized in the bending experiment were considered (Bossle et al., 2026).

Based on the results obtained using the tensile tests, mechanical properties of conventional SAE1010 steel were extracted from the scientific paper of Bossle et al. (2025) and entered into the software, as shown in Table 4.

Table 4: Mechanical properties entered into the SIMUFACT software.

Parameters	Material
Blank material	Conventional SAE1010 steel
Engineering Yield Stress, σ_e (MPa)	241.78
Maximum Stress, R_m (MPa)	343.56
Anisotropy Index, *r* (-)	1.067
Density, *ρ* (g/cm³)	7.85
Elasticity Modulus, *E* (GPa)	198.57
Poisson Coefficient, *v* (-)	0.29
Material Resistance Constant, *C* (MPa)	589.24
Hardening Index, *n* (-)	0.19
Coefficient of friction, (*μ*)	0.1

Source: Elaborated by authors (2026).

REMUNOM
ISSN 2178-6925

Received: 05/03/2026 - **Accepted:** 06/05/2026
Vol: 13.07
DOI: 10.66104/m4ev7706
Pages: 1-20

Figure 8 illustrates the initial (a) and final (b) positions of the punch, according to procedures established in the literature on numerical simulation of forming processes (Fu et al., 2010; Altan and Tekkaya, 2012).

Figure 8: Representation of the initial (a) and final (b) positions of the Punch.

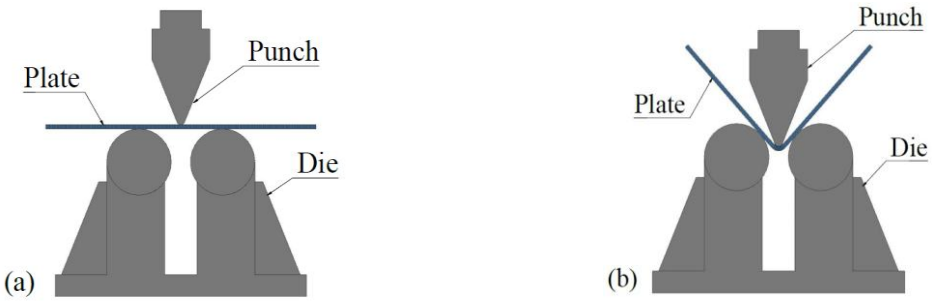

Source: Elaborated by authors (2026).

To mesh convergence, a 1mm general mesh size was adopted, hexahedral type elements, Sheetmesh mesh generator, quantity of elements 18900 and the number of elements along the thickness was 3 (Ledentsoy, et al., 2010).

3. Results and discussion

3.1 Experimental analysis

After the bending experiment, the True Strain (φ_x) values were verified in the outer bending region and in the length direction (x) of the test specimens, using the flexible and transparent ruler for measuring strains, as shown in Figure 9.

Figure 9: Verification of the True Strain (φ_x) of the bended outer region for the conventional SAE1010 steel of one of the specimens.

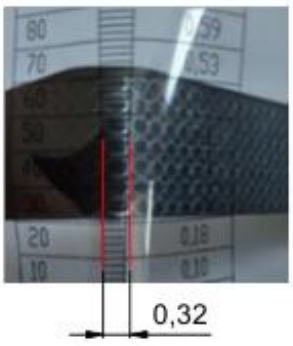

Source: Elaborated by authors (2026).

REMUNOM
ISSN 2178-6925

Received: 05/03/2026 - **Accepted:** 06/05/2026
Vol: 13.07
DOI: 10.66104/m4ev7706
Pages: 1-20

Table 5 presents the averages and standard deviations of the experimental values of True Strain (φ_x) in the outer bending region and in the length direction (x) for the conventional SAE1010 steel, as well as the record of the occurrence or not of cracks. As shown in Table 5, the average, standard deviations and average confidence intervals (95% CI) were calculated (Rodrigues and Iemma, 2014).

Table 5: The experimental values of True Strain (φ_x) in the outer bending region and in the length direction (x).

Material	Punch Radius r_p (mm)	Experimental True Strain φ_x (-)			Occurrence of fissures
		Average	Standard deviation	Confidence interval	
Conventional SAE1010 steel	3	0.32	0.006	0.32±0.004	no
	6	0.24	0.009	0.24±0.006	no
	9	0.18	0.007	0.18±0.005	no
	12	0.14	0.008	0.14±0.005	no

Source: Elaborated by authors (2026).

For conventional SAE1010 steel, in the outer bending region and for the group of test specimens with a Punch Radius (r_p) of 3mm, equal to the minimum specified by the DIN 9635 standard, of (1 to 3) times the initial thickness of the sheet (s_0), no cracks or fissures were observed, as well as for the groups of test specimens with Punch Radius (r_p) of 6, 9 and 12mm.

Looking at the results of the experiment for the conventional SAE1010 steel studied in this article, it was observed that the larger the Punch Radius (r_p), the smaller is the True Strain (φ_x) in the outer bending region and in the length direction (x), verified in the ellipses of the specimens through the visioplasticity method.

3.2 Analytical calculation method

Table 6 are shown the analytic values of True Strain (φ_x) in the outer bending region and in the length direction (x) for the conventional SAE1010 steel and were calculated using Equations 6 and 7, while the Midline Bending Radius (r_m) was calculated using Equation 8.

REMUNOM
ISSN 2178-6925

Received: 05/03/2026 - **Accepted:** 06/05/2026
Vol: 13.07
DOI: 10.66104/m4ev7706
Pages: 1-20

Table 6: Analytic values of True Strain (φ_x) in the outer bending region and Midline Bending Radius (r_m) for the conventional SAE1010 steel.

Material	Punch Radius r_p (mm)	True Strain φ_x (-) calculated (Eq. 6)	True Strain φ_x (-) calculated (Eq. 7)	Midline Bending Radius r_m (mm) (Eq. 8)
Conventional SAE1010 steel	3	0.35	0.29	4.5
	6	0.20	0.18	7.5
	9	0.14	0.13	10.5
	12	0.11	0.10	13.5

Source: Elaborated by authors (2026).

For reference, to compare with the results for conventional SAE1010 steel, Table 7 presents the values for the True Strain (φ_x) and the Midline Bending Radius (r_m) for the AHSS S900MC steel, obtained through analytical methods calculated using the Equations 6, 7, and 8, extracted of the work from Bossle et al. (2026).

Table 7: Analytic values of True Strain (φ_x) in the outer bending region and Midline Bending Radius (r_m) for the AHSS S900MC steel.

Material	Punch Radius r_p (mm)	True Strain φ_x (-) calculated (Eq. 6)	True Strain φ_x (-) calculated (Eq. 7)	Midline Bending Radius r_m (mm) (Eq. 8)
AHSS S900MC steel	3	0.35	0.29	4.5
	6	0.20	0.18	7.5
	9	0.14	0.13	10.5
	12	0.11	0.10	13.5

Source: Adapted and extracted from Bossle et al. (2026).

3.3 Computer simulation

Figure 10 shows the result of the computational numerical simulation of the True Strain (φ_x) in the outer bending region of conventional SAE1010 steel for a Punch Radius (r_p) of 6mm. In this simulation, it can be seen that the maximum True Strain (φ_x), with a value of 0.22, is located at the corners of the outer surface of the bending region and is shown in red.

REMUNOM
ISSN 2178-6925

Received: 05/03/2026 - **Accepted:** 06/05/2026
Vol: 13.07
DOI: 10.66104/m4ev7706
Pages: 1-20

Figure 10: Simulation of the True Strain (φ_x) of conventional SAE1010 steel for a Punch Radius (r_p) of 6 mm.

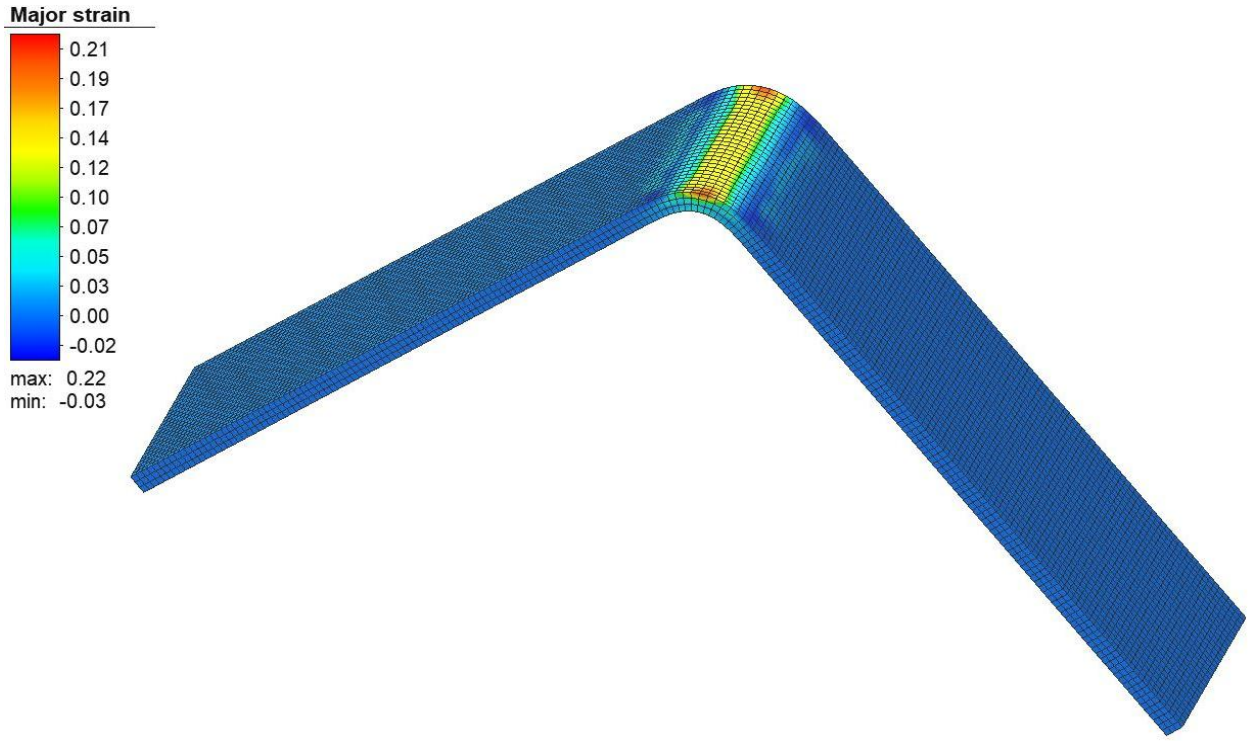

Source: Elaborated by authors (2026).

Table 8 presents the True Strain (φ_x) values in the outer bending region in the length direction (x) of the conventional SAE1010 steel studied here, obtained through computer simulation.

Table 8 : Computer simulation values for True Strain (φ_x) in the outer bending region and in the length direction (x) of the conventional SAE1010 steel.

Material	Punch Radius r_p (mm)	Computer simulation values for True Strain φ_x (-)
Conventional SAE1010 steel	3	0.29
	6	0.22
	9	0.17
	12	0.13

Source: Elaborated by authors (2026).

4. Discussion

The results of the experimental analysis in this work were considered a reference to make a comparative evaluation with the results of the analytical

REMUNOM
ISSN 2178-6925

Received: 05/03/2026 - **Accepted:** 06/05/2026
Vol: 13.07
DOI: 10.66104/m4ev7706
Pages: 1-20

methods and computer simulation to this steel.

The calculated average standard deviations and Confidence Intervals (CI 95%), close to zero for the measured average True Deformations (φ_x) and presented in Table 5, indicate homogeneity and a low risk of reading errors (Rodrigues and Iemma, 2014).

The comparative percentage of relative error of the results obtained through experimental analysis, analytical methods and computer simulation of the True Strain (φ_x) in the external bending region in the longitudinal direction (x) of conventional SAE1010 steel are shown in Figure 11.

Figure 11: Ratio between True Strain (φ_x) and Punch Radius (r_p) for the conventional SAE1010 steel.

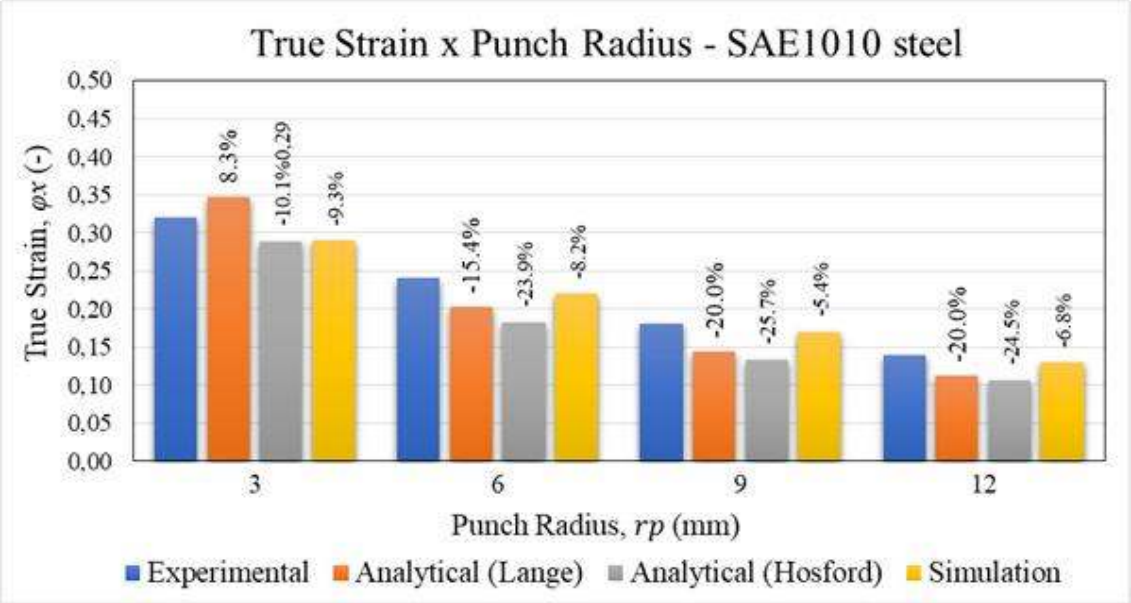

Source: Elaborated by authors (2026).

For conventional SAE1010 steel and the air bending process, as shown in the graph in Figure 10, differences occurred between the experimental results for True Strain (φ_x) in the external curvature region in the longitudinal direction (x). This is due to the different values of the parameters used in this experiment: Punch Radius (r_p), Distance between Supports (w) and Maximum Punch Displacement (h).

For the analytical method, using Equations 6 and 7, as shown in the graph in Figure 10, the values diverged significantly from those obtained by experimental

REMUNOM
ISSN 2178-6925

Received: 05/03/2026 - **Accepted:** 06/05/2026
Vol: 13.07
DOI: 10.66104/m4ev7706
Pages: 1-20

analysis, this is because both equations only used the variables Sheet thickness (s), Punch radius (r_p), and Midline Bending Radius (r_m) for the calculation, without considering other variables such as mechanical properties that could possibly influence the calculated results.

For values calculated and less than 10% those verified in the visioplasticity experiment, the observed deviation from the prediction may make the use of these two equations unfeasible, since the stress in the bending region may exceed the Maximum Stress (R_m) of the material.

Regarding the computer simulation, the graph in Figure 10 shows results below 10%, indicating that interactions with the software, such as the number of elements along the thickness, the quantity of elements, mesh size, and other simulation parameters, may have interfered with the results presented. However, for the sample sizes, the error percentages are considered acceptable (Rodrigues and Iemma, 2014).

According to the showed in the Table 6 and 7, although the conventional SAE1010 steel having different mechanical properties from AHSS S900MC steel, the analytical method shows that the values calculated using Equations 6 and 7 are the same for both steels, since the parameters considered in these equations are the Sheet Thickness (s), the Punch Radius (r_p) and the Midline Bending Radius (r_m).

Possibly due to its high ductility and its high capacity for absorbing plastic deformation, no cracks were observed in the outer bending region of the test specimens after the conventional SAE1010 steel bending experiment.

5. Conclusion

For conventional SAE1010 steel, the analytical calculation of true strain (φ_x) in the outer bend zone using Equations 6 and 7, the main methods currently available in the literature for air bending, showed significant discrepancies. Specifically, the calculated values deviated from the experimental results between -25.7% and 8.3%, suggesting that these equations may lead to inaccurate predictions for this type of steel. As shown in Table 6, these results are in agreement with previous studies on AHSS S900MC steel (Table 7). Consequently, for both conventional SAE1010 and

REMUNOM
ISSN 2178-6925

Received: 05/03/2026 - **Accepted:** 06/05/2026
Vol: 13.07
DOI: 10.66104/m4ev7706
Pages: 1-20

AHSS S900MC steel, there is a clear need to formulate a new equation that incorporates mechanical properties in the calculation of True Strain (φ_x).

In contrast, the results of the computational simulation using SIMUFACT FORMING 15® showed a difference of less than 10% compared to the experimental analysis. Therefore, the use of this software is recommended to predict the True Strain (φ_x) in conventional SAE1010 steel.

References

AERENS, R.; MASSELIS, S. Air bending. Scientific and Technical Research Center of the Metal Fabrication Industry (CRIF/WTCM/SIRRIS) MC 110, Leuven, Belgium, 2000.

ALMEIDA, I. Análise numérica e experimental da conformabilidade do aço SAE 1010 em chapas finas sem e com galvanização (gi-85). Dissertação de mestrado em engenharia mecânica, Pontifícia Universidade Católica de Minas Gerais, Belo Horizonte, 2021.

ALTAN, T.; TEKKAYA, A. Erman. *Sheet Metal Forming: Fundamentals*. Materials Park: ASM International, 2012.

AROLA, A-M.; KESTI, V.; RUOPPA, R. The effect of punch radius on the deformation of ultra-high strength steel in bending. Key Eng Mater 639: p. 139-146. 2015.

ASSOCIAÇÃO BRASILEIRA DE NORMAS TÉCNICAS. ABNT NBR ISO 7438: Materiais metálicos - Ensaio de dobramento. Rio de Janeiro: ABNT, 2022.

BOSSLE, V. de S.; SCHAEFFER, L.; RIFFEL, H. M.; ROCHA, R. P.; CHIARELLO, D.; TONIOLO, J. C. Análise do retorno elástico no processo de dobramento em V livre do aço SAE1010. Revista Derecho y Cambio Social. V. 22, n. 81, p. 01-15, 2025.

BOSSLE, V. de S.; SCHAEFFER, L.; RIFFEL, H. M.; ROCHA, R. P.; TONIOLO, J. C. Análise do Processo de Dobramento dos aços HSLA S700MC e AHSS S900MC. Revista Multidisciplinar do Nordeste Mineiro. V. 01-03, p. 01-24, 2026.

ÇAPAR, Y. Engineering Stress/Strain vs True Stress/Strain. URL https://yasincapar.com/engineering-stress-strain-vs-true-stress-strain/ – Access date 15.01.2026.

REMUNOM
ISSN 2178-6925

Received: 05/03/2026 - **Accepted:** 06/05/2026
Vol: 13.07
DOI: 10.66104/m4ev7706
Pages: 1-20

FARSI, M. A.; AREZOO, B. Bending Force and Spring-Back in V-Die-Bending of Perforated Sheet-Metal Components. Technical Papers • J. Braz. Soc. Mech. Sci. & Eng. 2011.

FOLLE, L. F.; et al. Escolha do Lubrificante Correto Torna Mais Precisa a Curva-limite de Conformação. Corte e Conformação de Metais. p. 64 - 76, 2008.

FU, Z.; MO, J.; CHEN, L.; CHEN, W. Using genetic algorithm-back propagation neural network prediction and finite-element model simulation to optimize the process of multiple-step incremental air-bending forming of sheet metal. Mater Des 31 (1):267-277, 2010.

HOSFORD, W.; CADDELL, R. Metal Forming Mechanics and Metallurgy. 4ª Ed., New York: Cambridge University Press, p. 30-37. 2011.

KLUGE, S. Prozesse der Blechumformung: Bauteil-, Werkzeug- und Fertigungsgestaltung im Karosseriebau. Munique. Carl Hanser Verlag, 2020.

LANGE, K. Handbook of metal forming. McGraw-Hill Book Company, New York, US, p. 723-755. 1985.

LEDENTSOY, D.; DÜSTER, A.; VOLK, W.; WAGNER, M.; HEINLE, I.; RANK, E. Model adaptivity for industrial application of sheet metal forming simulation. Finite Elem Anal Des 46 (7):585-600, 2010.

LIVATYALI, H.; ALTAN, T. “Prediction and elimination of Springback in straight flanging using computer aided design methods: Part 1”. Experimental Investigations. J. of Mat. Proc. Tech., Vol. 117(1-2), p. 262–268. 2001.

MITHU, M. A. H.; MOHAMMED.A. KARIM, M. A.; FERDOUS A. TAJ, F. A.; RAHMAN, A. Predicting springback in V-bending: Effects of load, load holding time, and heat treatment on common sheet-metal forming operations. Materials Today Communications. V. 43. 111668. 2025.

OEHLER, Gerhard; KAISER, Fritz. Schnitt-, Stanz- und Ziehwerkzeuge: unter besonderer Berücksichtigung der neuesten Verfahren und der Werkzeugstähle mit zahlreichen Konstruktions- und Werkstattbeispielen. 5 ed. Berlin: Springer-Verlag, 1973.

REMUNOM
ISSN 2178-6925

Received: 05/03/2026 - **Accepted:** 06/05/2026
Vol: 13.07
DOI: 10.66104/m4ev7706
Pages: 1-20

PERKA, A. *et al*. Advanced High-Strength Steels for Automotive Applicantions: Arc and Laser Welding Process, Properites, and Chalenges, Metals. V. 12, 2022.

ROCHA, R. P.; RIFFEL, M.; MOZETIC, H.; SCHAEFFER, L. Análise do Retorno Elástico no Processo de Dobramento em "V" em Aços de Alta Resistência. Brazilian Journal of Development. v.8, n.4, p. 27662-27677. Abril, 2022.

ROCHA, R. P.; RIFFEL; SCHAEFFER, L. Evaluation of Forming Limit Diagrams of Stainless Steel AISI 304 and AISI 430. Desenvolvimento em Questão. n.59, p. 1-18, 2023.

RODRIGUES, M. I.; IEMMA, A. F. Planejamento de experimentos e otimização de processos. 3ª ed. Campinas: Casa do Espírito Amigo Fraternidade Fé e Amor, 2014, p. 41-43. 2014.

RODRIGUES, J.; MARTINS, P. Tecnologia Mecânica: Tecnologia da deformação plástica - aplicações industriais. Lisboa: Escolar, p. 265-332, 2010.

SCHAEFFER, L.; NUNES, R. M.; BRITO, A. M. Tecnologia da estampagem de chapas metálicas. 1ª ed. Porto Alegre: Gráfica da UFRGS, p. 56-65. 2017.

TSCHÄTSCH, H. Praxiswissen Umformtechnik. Capter: 16 - Biegen. p. 164 – 181 Springer Book. 1997.

ULSAB. UltraLight Steel Auto Body – Advanced Vehicle Concepts (ULSAB-AVC). [homepage on the Internet] 2017: <http://www.worldautosteel.org/projects/ulsab-avc-2/>.

VORKOV, V. *et al*. Experimental Investigation of Large Radius Air Bending. The International Journal of Advanced Manufacturing Technology, V. 92. p. 3553-3569. 2017.

VORKOV, V. *et al*. Analytical Prediction of Large Radius Bending by Circular Approximation. Journal of Manufacturing Science and Engineering. V. 140, nº. 12. p. 121010-0 a 121010-12. 2018.